Available online at www.easd.procedia.org
EASD Procedia EURODYN (2026) 415-425

EASD Procedia

EURODYN 2026
XIII International Conference on Structural Dynamics
M. Beer, C. Papadimitriou, H. Jensen, J. Chen, M. Broggi, J. Behrensdorf (eds.)
Hannover, Germany, 27.09.–01.10 2026

MANUFACTURING OF A NONLINEAR QUASI-ZERO-STIFFNESS RESONATOR: FROM ADDITIVE MANUFACTURING TOWARDS INJECTION MOULDING

K. Steijvers[1,2] A. Karaman[1,2], R. F. Boukadia[2,3], D. R. Santo[4] , C. Claeys[2,3] , L.P.R. de Oliveira[4] and E. Deckers[1,2]

[1] KU Leuven, Campus Diepenbeek, Department of Mechanical Engineering
Wetenschapspark 27, 3950 Diepenbeek, Belgium
e-mail: kristof.steijvers@kuleuven.be

[2] Flanders Make@KU Leuven

[3] KU Leuven, Department of Mechanical Engineering
Celestijnenlaan 300B box 2420, 3001 Heverlee, Belgium

[4] Department of Mechanical Engineering, São Carlos School of Engineering, University of São Paulo, São Carlos, 13566-590, SP, Brazil

Keywords: Quasi-Zero-Stiffness, Injection Moulding, Locally Resonant Metamaterials

Abstract. *Locally resonant metamaterials enable combining lightweight design with favorable noise and vibration properties, allowing structures to meet ever tighter engineering requirements. Their superior vibration attenuation in targeted frequency zones emerges form the sub-wavelength addition of resonant elements to a host structure. Given their strong potential, numerous academic demonstrators have been realized. However, to advance these metamaterials to an industrially applicable engineering solution, both the manufacturing approaches and the tunable frequency range still form major hurdles. To date, the majority of locally resonant metamaterials are realized via additive manufacturing. While this technique can in particular cope with intricate metamaterial designs, it is not well-suited for cost-effective mass-manufacturing. To overcome this hurdle, injection moulding is recently explored and gaining increased attention to mass-manufacture metamaterials. This work investigates the potential of injection moulding to mass-manufacture a recently introduced quasi-zero-stiffness resonator, promising lower frequencies of vibration attenuation and a broadening of the frequency zone of attenuation due to the inherent nonlinear stiffness of the resonator. This resonant element consists of a dual-spring mechanism and an assembled buckled beam. First, the dual-spring mechanism is tailored to meet injection moulding manufacturing design guidelines after which the corresponding mould is designed. To allow design adaptation, the beam is 3D printed and the influence of the beam dimensions on the resonator performance is experimentally assessed together with the repeatability of the assembled system.*

ISSN:2311-9020 © 2026 The Authors. Published by EASD Procedia.
Peer-review under responsibility of the Organizing Committee of EURODYN 2026.
doi: 10.47964/1326.10670.334

1 INTRODUCTION

The pursuit of lightweight structures with superior vibration and acoustic performance has led to increasing interest in locally resonant metamaterials. In these systems, resonant elements are attached to a host structure at a sub-wavelength scale, enabling the emergence of frequency bands in which global vibration suppression can be achieved [1]. Despite their significant potential, the practical implementation of such metamaterials remains challenging, as their manufacturability is often limited and their performance is typically restricted to narrow frequency bands, hindering industrial applicability.

Injection moulding (IM) has been identified as a cost-effective manufacturing technique for metamaterials, as demonstrated in several scientific studies [2],[3],[4]. In addition to its scalability, the process offers opportunities to predict the influence of manufacturing parameters on the vibro-acoustic performance of the resulting structures, thereby enabling the production of targeted designs without extensive iterative tuning [5]. To enhance bandwidth and tunability, various strategies have been explored, including the incorporation of concentrated masses or damping, often through multi-material realizations [6], [7]. However, further lowering the operational frequency range while maintaining broadband performance remains a key challenge. In this context, nonlinear solutions provide an elegant alternative [8], as reducing stiffness in linear systems may lead to structural instabilities.

Among the variety of nonlinear approaches, quasi-zero-stiffness (QZS) designs have received considerable attention [9], [10]. These systems enable a significant reduction in effective stiffness without compromising structural stability, thereby allowing low-frequency vibration isolation. However, existing QZS implementations often rely on complex assemblies, which increase complexity and manufacturing cost [11], [12]. Furthermore, predicting their performance during the design phase remains challenging, as it typically relies on simplified lumped-parameter analytical models that lack direct linkage to material properties and geometric design parameters [10],[13],[14]. This further complicates the accurate incorporation of manufacturing-induced effects, which are typically predicted numerically. As a result, the direct translation of design models to manufactured QZS systems remains nontrivial.

This work investigates the potential of IM for the fabrication of a quasi-zero-stiffness resonator, based on the design proposed in [15]. The manufacturing process influences on the design are assessed by geometrical measurements whereafter the design is further tailored for optimal QZS performance. Last, the repeatability of the realization approach (manufacturing process and assembly) are assessed by manufacturing multiple samples and measuring their static performance after multiple repetitions of assembly to assess the practical implementation potential of the design. In Section 2, the resonator design is tailored for IM manufacturing supported by IM process simulations while an efficient assembly method is foreseen. Section 3 explains the manufacturing and measurement procedures after which the results are discussed in Section 4. The main conclusions and steps for future work are discussed in Section 5.

2 RESONATOR AND MOULD DESIGN

The injection moulding process is briefly discussed, whereafter the main design changes for mouldability are highlighted and supported by numerical process simulations. Next the mould and assembly design are further detailed.

2.1 The injection moulding process

Starting from polymer granulates which are fed into a heated barrel, the rotating motion of a reciprocating screw melts and homogenizes a specified amount of polymer material (dosing

phase). Next, the screw injects this material into the mould cavity at a specified flow rate. When the cavity is nearly filled, the injection phase transitions to pressure regulation, filling the remainder of the cavity while simultaneously compensating for material shrinkage in the cooled mould by applying the packing pressure. When the polymer is solidified, the screw moves backward and doses the next shot of material while the product further cools down. Last, the mould opens and the product is ejected, often by moving pins inside of the mould after which the whole cycle repeats.

2.2 Dual-spring design

The initial resonator design proposed in [15] (Figure 1a) is assembled from three different components. A v-shaped outer spring, an eight-shaped inner spring and a straight beam connecting both springs, which is pre-loaded by the v-shaped spring when assembled. This preload causes the beam to buckle, while it is being kept in position by the eight-shaped inner spring. These effects together cause the desired nonlinear response. In view of mass-manufacturing via injection moulding, the initial design is tailored. First, the number of components is reduced, limiting the number of required moulds. Therefore, the v-shaped spring and eight-shaped inner spring are combined to one component as of now referred to as dual spring. Simultaneously, the v-shape is widened and the inner spring is aligned creating a more 2D, mouldable component (Figure 1b). To comply with IM design guidelines, wall thickness should be as uniform as possible, and can only be changed gradually over the design. Additionally, thin sections cannot be followed by thicker sections since the polymer flow will be blocked by the already solidified thin section, leading to voids or even unfilled products. Based on these requirements, the design is finalized (Figure 1c).

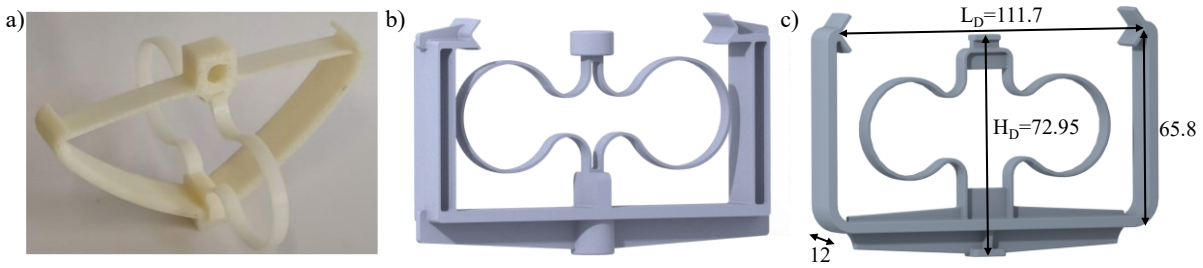


Figure 1: a) Initial additive manufactured design proposed in [15], b) first design iteration of the dual-spring for IM manufacturing and c) final dual-spring mechanism design.

To support these design changes related to mouldability, a numerical IM process simulation is performed in Moldex3D commercial software [7]. This way, the filling, packing and cooling behavior of the resonator during moulding are predicted together with the resulting part warpage, while accounting for material pressure–specific volume–temperature (pvT), viscosity and process settings. To this end, the design is discretized with a 5 layer boundary layer mesh with an element size of 1 mm. ABS Novodur p2H-AT from Ineos [16] material was assigned based on its excellent flow behavior and mouldability. Rule of thumb processing conditions have been set for this initial simulation: melt temperature of 240 °C, mould temperature of 60 °C, injection flow rate of 30 cm^3/s and a packing pressure of 70% of the maximum injection pressure is set for 10 seconds.

The thin sections of the first design iteration clearly solidify early in the moulding process, preventing further filling and shrinkage compensation in the top parts by the packing pressure

(Figure 2a). Furthermore, a displacement of 1.5 mm on both sides (3 mm in total) occurs due to shrinkage and resulting warpage. For the adjusted final design (Figure 2b), the uniform wall thickness causes more uniform solidification over the entire design, allowing sufficient shrinkage compensation by the packing pressure as the thin sections are only solidified after 6 seconds. This way, the overall displacement after moulding is reduced by 50 %.

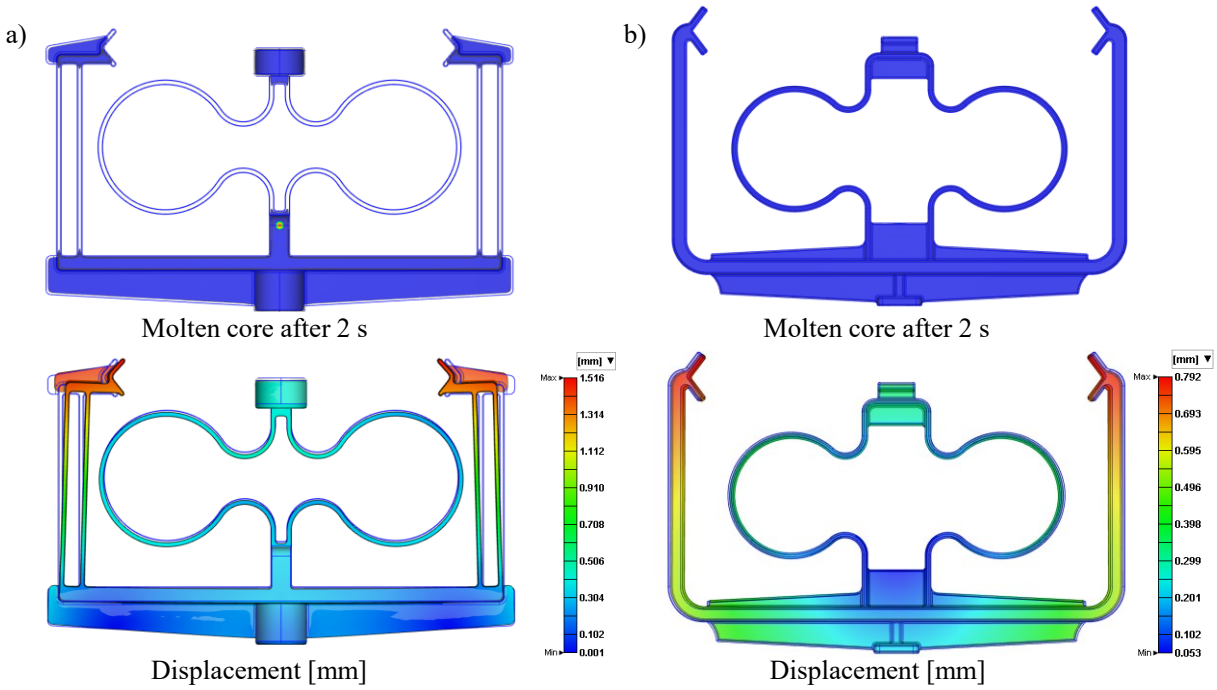


Figure 2: Molten core after 2 seconds of cooling (purple) and final displacement caused by shrinkage and warpage for the a) first design iteration and b) the final design.

2.3 Mould design

To manufacture the resonator, a mould with replaceable cavity inserts is used. This allows for the flexible manufacturing of multiple products from the same mould base. Given the resonator's depth of 12 mm, two inserts with a cavity depth of 6 mm are placed in the fixed and moving mould side respectively. This reduces the required machining depth per cavity, facilitating mould manufacturing. An asymmetric draft angle of 1.5 and 2 degrees are foreseen in the moving and fixed side, respectively to ensure the part remains in the moving mould side during mould opening. Last, 30 ejector pins are added to ensure proper demoulding of the part.

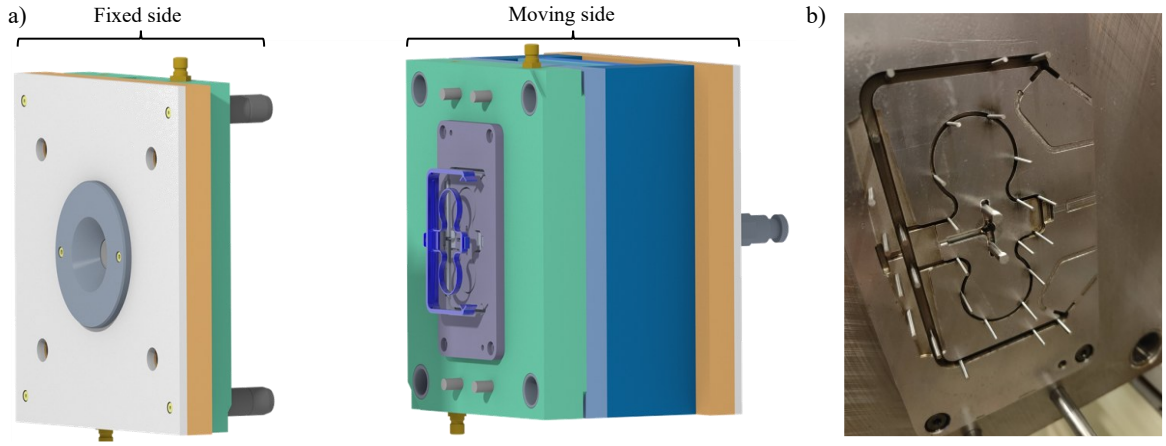


Figure 3: a) overview of the mould, b) part cavity in the moving mould side with moved forward ejector pins.

2.4 Beam design

To achieve the QZS behavior, a straight beam is separately manufactured at overlength, providing the required buckling effect when assembled to the inner spring of the moulded dual-spring mechanism (Figure 4). To this end, a dove tail connection is foreseen. The nonlinear force displacement relation of the resonator is expected to be highly sensitive to the interplay between the beam and dual-spring part dimensions. Since altering the dimensions of a moulded part is cost intensive as it requires manufacturing a new mould cavity, it was decided in a first step to manufacture the beam via 3D-printing. This enables to experimentally evaluate the influence of the beam dimensions on the force-displacement relation of the device.

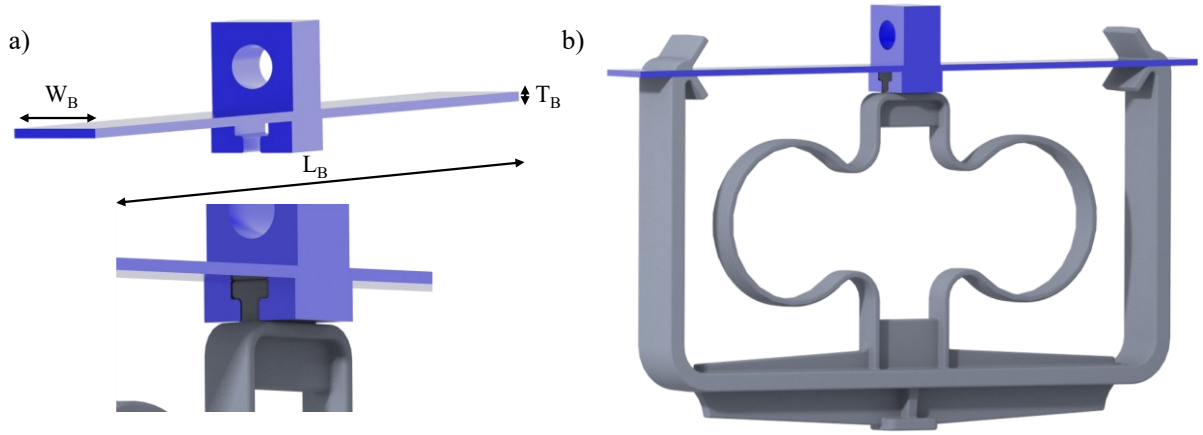


Figure 4: a) Beam design and main dimensions, b) final assembly of the nonlinear resonator.

3 RESONATOR MANUFACTURING AND EXPERIMENTAL CHARACTERIZATION

An electrical DEMAG ERGOTECH IntElect 50/330-100 IM machine with a 22 mm horizontal screw and a maximal mould clamping force of 500 kN is used to manufacture the dual-spring device (Figure 5a). The same rule of thumb process parameters as those used in the simulation are applied. The beams are manufactured using a Bambulab x1 Carbon 3D printer and Bambu ABS filament.

First, 15 beams are manufactured (Figure **5**b) with different length L_B, width W_B or thickness T_B in order to experimentally assess the influence of the beam dimensions (Figure 4) on the QZS plateau of the force-displacement relation (Table 2). The main dimensions are measured using a caliper with a resolution of 0.01 mm. To experimentally characterize the force-displacement relation, a Zwick BZ2.5/TS1S tensile testing machine is used, equipped with an AST KAF-W Force transducer with a maximum force of 500 N and a relative accuracy of 0.05 % (Figure **5**c). The samples are conditioned at 23 °C and 60% humidity for 48 hours before testing. Based on these outcomes, an optimal beam length is selected after which three more resonators are manufactured and assembled. For these resonators, the force-displacement relation is measured twice after assembly, after which the samples are kept assembled for 48 h to investigate the influence of creep on the static performance of the resonators.

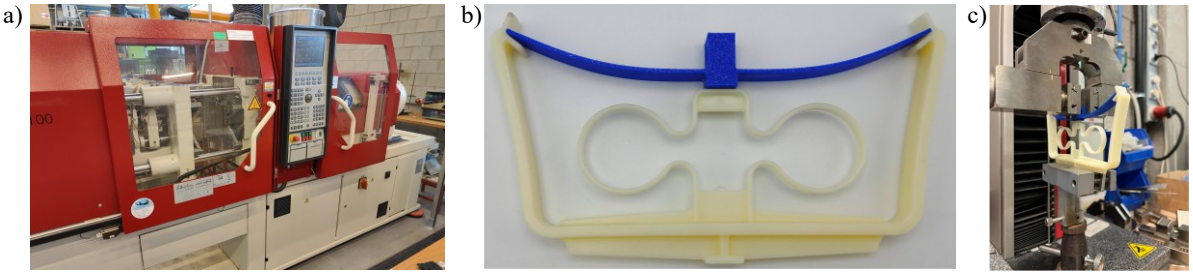


Figure 5: a) Electrical injection moulding machine, b) manufactured beam and spring mechanism assembled together, c) quasi-static force-displacement measurement of the resonator.

4 RESULTS AND DISCUSSION

The dimensional measurements on the moulded dual-spring mechanism and the 3D printed beam are discussed and compared to predicted dimensions in Moldex3D. Next, the static force-displacement repeatability of the inner spring is assessed from tensile tests, together with the influence of the beam dimensions on the QZS plateau. Last, the assembly and time dependence of the static resonator performance are assessed.

4.1 Dimensional measurements

The dimensional measurements of the injection moulded dual-spring device (Table 1) show low variability over the 15 samples with a standard deviation of only 0.4 mm and 0.1 mm for the L_D and H_D parameter respectively (Figure **1**). As compared to the CAD design, the manufactured resonators show slightly smaller dimensions caused by the polymer shrinkage. For the amorphous ABS material, shrinkage is smaller as compared to semi-crystalline polymers and typically determined from the materials pvT relation at around 0.65 percent [16]. For this design, the length L is decreased from 111.7 mm to 109.7 mm or 1.8 percent. This indicates warpage in the part, bending the upward standing beams towards each other and so causing a decrease of L_D. This effect is better predicted in the Moldex3D process simulation, leading to a predicted length and height of 110.06 mm and 72.36 mm. This illustrates the potential of incorporating IM process simulations during the future development of a modelling framework for QZS devices [5].

Dual-spring						
	Length L_D [mm]			Height H_D [mm]		
Sample nr.	CAD	Moldex3D	Measured	CAD	Moldex3D	Measured
L135	111.7	110.06	109.7	72.95	72.36	71.5
L136	111.7	110.06	109.6	72.95	72.36	72
L137	111.7	110.06	110	72.95	72.36	71.5
L138	111.7	110.06	111	72.95	72.36	71.5
L139	111.7	110.06	109.6	72.95	72.36	71.5
L140	111.7	110.06	109.5	72.95	72.36	71.5
L141	111.7	110.06	109.7	72.95	72.36	71.6
W10	111.7	110.06	109.4	72.95	72.36	71.6
W11	111.7	110.06	109.6	72.95	72.36	71.5
W13	111.7	110.06	109.5	72.95	72.36	71.5
W14	111.7	110.06	109.5	72.95	72.36	71.8
T1.1	111.7	110.06	109.4	72.95	72.36	71.5
T1.2	111.7	110.06	109.3	72.95	72.36	71.7
T1.4	111.7	110.06	110.2	72.95	72.36	71.5
T1.5	111.7	110.06	109.5	72.95	72.36	71.5
AV			109.7			71.6
STDEV			0.4			0.1

Table 1: Dimensional measurements of the injection moulded dual-spring.

Beam						
	L_B [mm]		W_B [mm]		T_B [mm]	
Sample nr.	CAD	Measured	CAD	Measured	CAD	Measured
L135	135	134.45	12	11.9	1.3	1.3
L136	136	135.5	12	11.9	1.3	1.3
L137	137	136.5	12	11.9	1.3	1.3
L138	138	137.5	12	11.9	1.3	1.3
L139	139	138.6	12	11.9	1.3	1.3
L140	140	139.55	12	11.9	1.3	1.3
L141	141	140.5	12	11.9	1.3	1.3
W10	138	137.5	10	9.95	1.3	1.3
W11	138	137.5	11	11	1.3	1.3
W13	138	137.5	13	13	1.3	1.3
W14	138	137.5	14	14	1.3	1.3
T1.1	138	137.5	12	11.9	1.1	1.15
T1.2	138	137.5	12	12	1.2	1.2
T1.4	138	137.5	12	11.9	1.4	1.4
T1.5	138	137.5	12	11.9	1.5	1.5

Table 2: Dimensional measurements of the 3D printed beam.

In accordance with the moulded samples, the 3D printed beam dimensions (Table 2) show shrinkage, leading to the largest absolute dimensional changes in the length and width direction. As the beam is a flat 2D geometry, warpage is less pronounced, reducing the dimensional mismatch between the CAD and manufactured part.

4.2 Stiffness measurements

The force-displacement relation of the inner spring of the injection moulded part (Figure 6a) shows consistent and linear behavior in the measured displacement range for all 15 samples. The slope of the curves has been calculated at 0.41 N/mm with a standard deviation of only 0.0028 N/mm, proving the high repeatability of the IM process. When assembling the different beams to the corresponding linear spring system (Figure 6b), nonlinear behavior of the assembly is observed, due to the buckling movement of the beam, balanced by the moulded dual-spring system. As expected, the static response of the design is highly sensitive to small changes in the beam geometry. For increasing beam lengths, a zone of decreased stiffness is observed (sample L_{135}-L_{138}). For a beam length of 139-140 mm a nearly flat plateau is observed between 5-15 mm displacement, corresponding to the desired QZS behavior. When the length is further increased, negative stiffness is achieved (sample L_{141}). In case of changing the beam width and thickness for a beam length of 138 mm, similar effects can be achieved. This showcases that the beam buckling governs the static response of the system, and care should be taken to achieve consistent manufactured beams in order to have the correct interplay with the moulded dual-spring mechanism to achieve the desired nonlinear behavior.

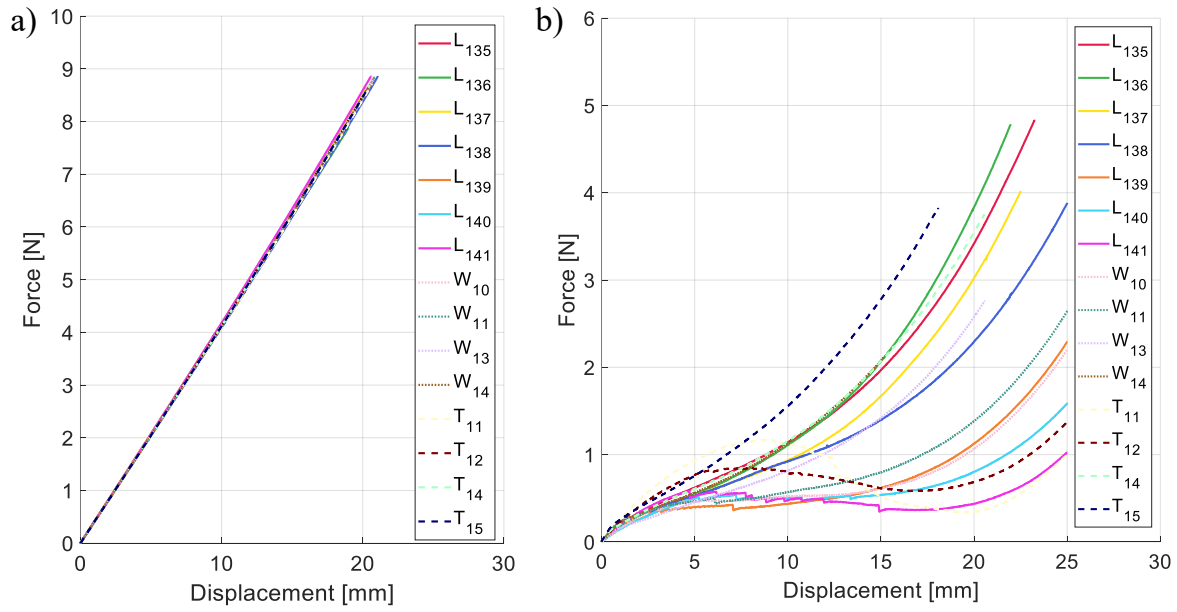


Figure 6: Force-displacement curves of the a) linear inner spring of the injection moulded dual-spring mechanisms, b) assembled nonlinear resonator with different beam lengths, widths and thicknesses.

4.3 Assembly-induced variability and time dependance

When manufacturing three different assemblies from the same nominal beam design (L=139 mm, W=12 mm and T=1.3 mm), the force displacement curves after the first assembly step (Figure 7, red) show highly corresponding behavior for the different designs. When reassembling the beam, no significant influence on both the linear as the nonlinear force-

displacement relation is observed, proving the robustness of the assembly mechanism. When leaving the system assembled for 48h, a clear increase in force is measured for the assembled system. When assembled for longer times, creep in the buckled beam causes the nonlinear buckling effect to be less-pronounced, deteriorating the zone of QZS. It was observed that the small thickness of 1.3 mm causes zones of plastic deformation on the beam, which potentially can be reduced by increasing its thickness while simultaneously decreasing its width to achieve the desired QZS result.

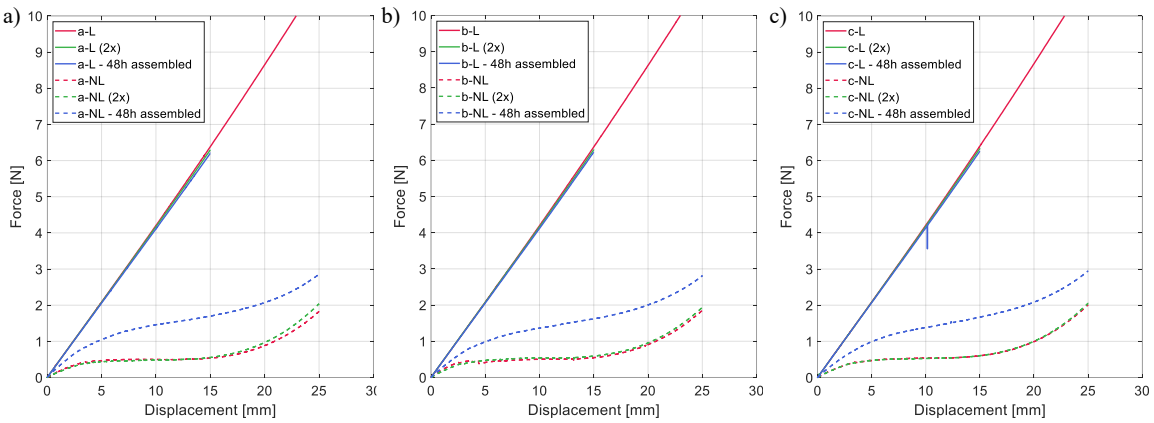


Figure 7: Force-displacement curves of three different nonlinear resonator assembly systems (a, b and c, respectively) measured for two immediate (dis)-assembly steps and after being assembled for 48 hours.

5 CONCLUSION

QZS devices show high potential for achieving low-frequency vibration reduction in locally resonant metamaterials. The manufacturing of these intrinsic highly sensitive systems is challenging, as most designs consist of multiple components, and manufacturing greatly influences the final performance. This work details the design and manufacturability assessment of an IM dual-spring device which, together with a 3D printed buckling beam, achieves QZS behavior. It is shown that moulding simulations allow for accurate prediction of the final part geometry, which is important to ensure correct interplay between the different assembly components in order to achieve the desired QZS performance. The moulded dual-spring mechanism shows repeatable dimensions and quasi-static behavior, whereas the beam dimensions allow the tuning of the final resonator response, accounting for the manufacturing effects of the dual-spring mechanism. Last, the assembly mechanism is found not to influence the static resonator response while creep effects affect the response over time and should be reduced. Next steps include the development of a finite element based modelling framework, in which IM process simulation results can be accounted for. Moreover, a mould design for the beam will be foreseen whereafter dynamic response measurement of a fully injection moulded system can be executed.

6 ACKNOWLEDGEMENTS

The research of K. Steijvers (fellowship no. 1S63423N) is funded by a grant from the Research Foundation – Flanders (FWO). The European Commission is gratefully acknowledged for their support of the METAVISION research project (GA 101072415). Views and opinions expressed are, however, those of the authors only and do not necessarily reflect those of the European Union. The European Union cannot be held responsible for them. The Research Foundation Flanders (FWO) and São Paulo Research Foundation- Brazil (FAPESP) are grate-

fully acknowledged for their support through the bilateral research cooperation project (FWO no. G0F9922N, FAPESP no. 21/05510-3). Internal Funds KU Leuven are gratefully acknowledged for their support.

REFERENCES

[1] Claeys,C., K. Vergote, P. Sas, and W. Desmet, "On the potential of tuned resonators to obtain low-frequency vibrational stop bands in periodic panels," *J. Sound Vib.*, vol. 332, no. 6, pp. 1418–1436, Mar. 2013, doi: 10.1016/j.jsv.2012.09.047.

[2] Wang,X., P. Sun, X. Gu, S. Xu, X. Luo, and Z. Huang, "Industrial-scale manufactured acoustic metamaterials for multi-bandgap sound reduction," *Int. J. Mech. Sci.*, vol. 293, p. 110184, May 2025, doi: 10.1016/J.IJMECSCI.2025.110184.

[3] Chojnacka,K., A. Kras, and T. Kamisinski, "Sound transmission loss dip compensation using multi_resonant vibroacoustic metamaterial designed for injec_tion moulding.,"

[4] Yu,J., C. Nerse, G. Lee, S. Wang, and C. Kyoung-Jin, "Mass production applicable locally resonant metamaterials for NVH applications," in *Proceedings of the 26th International Congress on Sound and Vibration, ICSV 2019*, 2019.

[5] Steijvers,K., C. Claeys, L. Van Belle, and E. Deckers, "Incorporating Manufacturing Process Simulations to Enhance Performance Predictions of Injection Moulded Metamaterials," *J. Vib. Eng. Technol. 2023*, vol. 1, pp. 1–13, Oct. 2023, doi: 10.1007/S42417-023-01159-1.

[6] Stejivers,K., S. Govaerts, C. Claeys, L. Van Belle, and E. Deckers, "Broadening the vibration attenuation of locally resonant metamaterials using multi-material injection moulding," *J. Vib. Acoust.*, vol. 148, no. 2, pp. 1–18, Apr. 2025, doi: 10.1115/1.4070715/1229462.

[7] Pires,F., M. Wandel, C. Thomas, E. Deckers, W. Desmet, and C. Claeys, "Improving the Sound Transmission Loss of an Aircraft Ceiling Panel by Locally Resonant Metamaterials," in *SAE Technical Papers*, SAE International, 2022. doi: 10.4271/2022-01-0960.

[8] Hao,R. B., Z. Q. Lu, H. Ding, and L. Q. Chen, "A nonlinear vibration isolator supported on a flexible plate: analysis and experiment," *Nonlinear Dyn.*, vol. 108, no. 2, pp. 941–958, Apr. 2022, doi: 10.1007/S11071-022-07243-7.

[9] Sheng,P., S. Jing, and Z. Zhang, "On the Characteristics and Practical Parameters Selection of a Quasi-Zero-Stiffness Isolator," *Int. J. Struct. Stab. Dyn.*, vol. 22, no. 15, Jun. 2022, doi: 10.1142/S0219455422501723.

[10] Noh,J., Y.-J. Yoon, P. Kim, J. Noh, Y.-J. Yoon, and P. Kim, "Anhysteretic high-static-low-dynamic stiffness vibration isolators with tunable inertial nonlinearity", doi: 10.1007/s11071-023-09179-y.

[11] Tian,Y., D. Cao, Y. Wang, J. Tang, and B. Jiang, "A Study of a Pendulum-Like Vibration Isolator With Quasi-Zero-Stiffness," *J. Comput. Nonlinear Dyn.*, vol. 17, no. 5, May 2022, doi: 10.1115/1.4053406/1133368.

[12] Xu,K., M. Niu, Y. Zhang, and L. Chen, "An active high-static-low-dynamic-stiffness vibration isolator with adjustable buckling beams: theory and experiment," *Appl. Math. Mech. (English Ed.*, vol. 45, no. 3, pp. 425–440, Mar. 2024, doi: 10.1007/S10483-024-3087-6/METRICS.

[13] Huang,X., X. Liu, J. Sun, Z. Zhang, and H. Hua, "Effect of the system imperfections on the dynamic response of a high-static-low-dynamic stiffness vibration isolator," *Nonlinear Dyn.*, vol. 76, no. 2, pp. 1157–1167, Jan. 2014, doi: 10.1007/S11071-013-1199-7

[14] Liu,C. and K. Yu, "Design and experimental study of a quasi-zero-stiffness vibration isolator incorporating transverse groove springs," *Arch. Civ. Mech. Eng.*, vol. 20, no. 3, pp. 67-, Sep. 2020, doi: 10.1007/S43452-020-00069-3

[15] D.R. Santo, E. Deckers, C. Claeys, R.F. Boukadia, and L.R.P. de Oliveira, "Improving the low-frequency vibration performance of meta- materials with high-static-low-dynamic stiffness local resonators ," in *Proceedings of ISMA 2024 - International Conference on Noise and Vibration Engineering and USD 2024 - International Conference on Uncertainty in Structural Dynamics*, 2024, p. 11.

[16] "NOVODUR P2H-AT - Novodur® favorable buying at our shop." [Online]. Available: https://www.ineos-styrolution.com/Product/Novodur_Novodur-P2H-AT_SKU401200140442.html